A New Control Strategy for DFIG Wind Farm with VSC-HVDC Integration

YONG LIAO, GUODONG WANG*
State Key Laboratory of Power Transmission Equipment & System Security and New Technology
Chongqing University
No. 174 Shazheng Street, Shapingba District, Chongqing, 400044, China
CHINA
*Corresponding author {wgdonline@163.com}

Abstract: - This paper proposes a new control strategy for a doubly-fed induction generator (DFIG) wind farm with VSC-HVDC integration to ensure a secure and reliable operation of the whole system. Based on a virtual voltage orientation, a steady-state voltage control block and a dynamic voltage control block with a cross-product term of d-q currents are separately designed for wind-farm-side VSC (WFVSC) to control the wind farm voltage. Meanwhile, with the consideration of ac and dc side parameters variation and external disturbance, an improved backstepping control scheme with Lyapunov stability proof is designed for the grid-side VSC (GSVSC). To validate the proposed control strategy, three different simulation cases with consideration of system parameters variation and external disturbances are introduced, and numerical simulation results for a 200MW DFIG wind farm with VSC-HVDC integration confirm that the proposed control strategy is of great satisfactory operation performance.

Key-Words: - Doubly fed induction generator (DFIG), voltage source converter (VSC), high voltage dc transmission (HVDC), wind farm, backstepping, Power quality

1 Introduction

The ratings of modern wind farms are increasing rapidly in the term of planning, construction and operation around the world, however, much of them are remote located from the power grid, especially for the emerging offshore wind farms. The integration of these large wind farms to the grid over distances of tens of kilometres creates a number of technical, commercial, and environmental challenges for the developers and system operators [1-2]. Conventionally, the high voltage ac (HVAC) transmission with its low cost and relatively simple layout has been widely used. However, the large amounts of capacitive current in the long ac cables significantly reduce the cable transmission capacity [3]. On the other hand, the traditional line-commutated converter high voltage dc (LCC-HVDC) [4-5] using thyristors needs an external commutation voltage for working properly, which hinders its application to weak ac system. In recent years, voltage-source converter HVDC (VSC-HVDC) using IGBT has attracted increasing attention for that it offers some advantages such as no external voltage source need for commutation, independent active and reactive power control, etc [6]. With these merits, a number of VSC-HVDC installations are constructed and now in operation, including the integration of renewable energy with this transmission [7]. In China, the East China Sea Bridge offshore wind farm project is a pilot exploration of renewable energy with this integration. Therefore, it is necessary to study the control strategy for the wind farm with VSC-HVDC integration and investigate its corresponding interactions between wind farms and the connected grid to ensure a secure and reliable operation of the whole system.

Although the control strategies for VSC-HVDC with two independent power grids have been well documented, the control study on wind farm with VSC-HVDC grid integration is really another new case. Generally, independent control strategy with different control objects are separately designed for the wind-farm-side VSC (WFVSC) and grid-side VSC (GSVSC). As for the WFVSC control design, a clear and simple voltage magnitude controller [6, 8] is usually used, however, since there is no current control scheme, the dynamic performance is unsatisfied and the current limitation can only be achieved by an indirect method. Moreover, in practice, there may exist a power demand near the wind farm, such as offshore oil platform [9], hence, the impact of local load to the control performance of WFVSC still needs further study. Additionally,

the system parameters variation also needs consideration as they are changing due to the fluctuation of wind power, transformer saturation, line aging, etc [10]. On the other hand, the GSVSC is designed to control the dc-link voltage and output the wind power to the grid. Since the GSVSC is a nonlinear and coupled structure, many different nonlinear control strategies [10-13] are designed to improve the operation performance. In recent years, backstepping control design techniques have received great attention because of its systematic and recursive design methodology for non-linear feedback control [13-15]. In [13], the backstepping control scheme is designed for VSC-HVDC with two independent power systems. However, the possible occurrence of uncertainties caused by the capacitance parameters and external disturbances were not considered.

In this study, a new control strategy is proposed for a wind farm with VSC-HVDC integration to ensure a secure and reliable operation of the whole system. In order to improve the performance of wind farm voltage, a steady-state voltage control block and a dynamic voltage control block with a cross-product term of d-q currents are designed for WFVSC. Meanwhile, with consideration of ac/dc-side parameters variation and external disturbance, an improved backstepping control scheme with Lyapunov stability proof is designed for GSVSC. In addition, since the doubly fed induction generator (DIFG) is employed by many new wind farms for its advantages over others [1], a DFIG wind farm is applied in this study. The rest of the paper is organized as follows. Section 2 gives the whole dynamic model descriptions. The principles of the proposed control strategy are discussed in Section 3. Simulation results for three different cases are provided in Section 4, and finally, Section 5 draws the discussions and conclusions.

2 System dynamic model descriptions

2.1 System descriptions

The entire configuration of the DFIG wind farm with VSC-HVDC integration is depicted in Fig. 1, which consists of a DIFG wind farm, a wind-farm-side filter, a wind-farm-side voltage source converter (WFVSC), a high voltage dc bus, a grid-side VSC (GSVSC), a grid-side filter as well as the transformers on the two sides. Considering that there may be exist a power demand of local load,

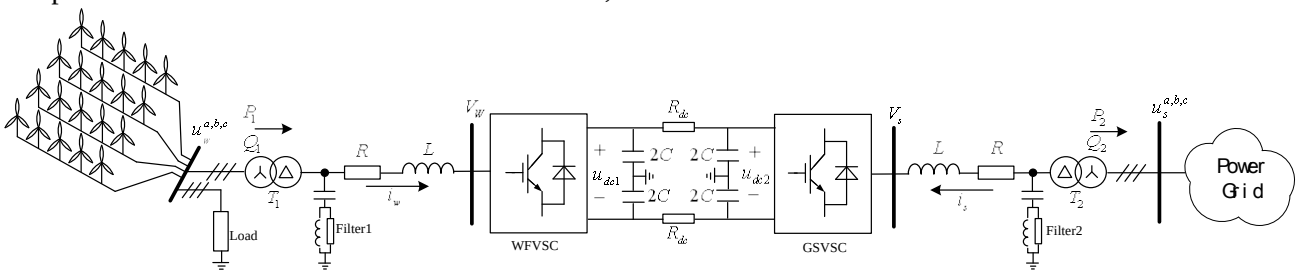

Fig.1. Schematic diagram of DFIG wind farm with VSC-HVDC integration

thus, a local load is contained in the system configuration and its impact on the system control performance will be discussed in the following study.

2.2 WFVSC dynamic model descriptions

The dynamic equations for WFVSC under the synchronous d-q reference frame rotating at an angular velocity of ω_w can be written as:

$$\begin{cases} L_w \dfrac{\mathrm{d}i_{wd}}{\mathrm{d}t} = -R_w i_{wd} + \omega_w L_w i_{wq} - v_{wd} + u_{wd} \\ L_w \dfrac{\mathrm{d}i_{wq}}{\mathrm{d}t} = -R_w i_{wq} - \omega_w L_w i_{wd} - v_{wq} + u_{wq} \end{cases} \quad (1)$$

Where (u_{wd}, u_{wq}) and (i_{wd}, i_{wq}) are d-axis and q-axis voltages and currents of the wind farm grid; v_{wd} and v_{wq} are d-axis and q-axis ac voltages of the WFVSC; R_w and L_w are the equivalent resistors and inductors within transmission lines between the WFVSC and the wind farm, including the transformer T1; ω_w is the electric angular frequency of the wind farm grid.

The corresponding complex vector equivalent circuits for ac side of WFVSC in the synchronous reference frame rotating at an angular velocity of ω_w is shown in Fig. 2.

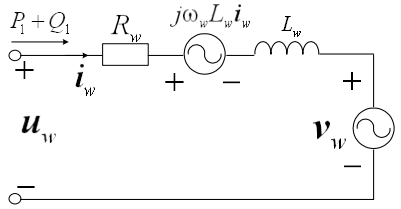

Fig. 2. Equivalent circuits of WFVSC in the synchronous reference frame.

The WFVSC dynamic model (1) can be rewritten in the stable state as

$$\begin{cases} u_{wd} = R_w i_{wd} - \omega_w L_w i_{wq} + v_{wd} \\ u_{wq} = R_w i_{wq} + \omega_w L_w i_{wd} + v_{wq} \end{cases} \quad (2)$$

The corresponding stable d-q voltage components of the wind farm grid can be calculated according to equation (2), when the wind farm is well controlled and operating at the given voltage.

2.3 GSVSC dynamic model descriptions

Similarly, the dynamic equations for GSVSC [16] under the synchronous d-q reference frame rotating at a synchronous angular ω_s velocity of can be written as:

$$\begin{cases} L_s \dfrac{\mathrm{d}i_{sd}}{\mathrm{d}t} = -R_s i_{wd} + \omega_s L_s i_{sq} - v_{sd} + u_{sd} \\ L_s \dfrac{\mathrm{d}i_{sq}}{\mathrm{d}t} = -R_s i_{wq} - \omega_s L_s i_{sd} - v_{sq} + u_{sq} \end{cases} \quad (3)$$

Where (u_{sd}, u_{sq}) and (i_{sd}, i_{sq}) are d-axis and q-axis voltages and currents of the wind farm grid; v_{sd} and v_{sq} are d-axis and q-axis ac voltages of the GSVSC; R_s and L_s are the equivalent resistors and inductors within transmission lines between the GSVSC and the wind farm, including the transformer T2; ω_s is the electric angular frequency of the power grid. Moreover, the active and reactive power for GSVSC can be represented as

$$\begin{cases} P_2 = -1.5(u_{sd} i_{sd} + u_{sq} i_{sq}) \\ Q_2 = -1.5(u_{sq} i_{sd} - u_{sd} i_{sq}) \end{cases} \quad (4)$$

On the other hand, the dynamic model of the dc side of the GSVSC can be described as

$$\frac{du_{dc2}}{dt} = -\frac{1.5\eta(u_{sd} i_{sd} + u_{sq} i_{sq})}{C u_{dc2}} + \frac{i_{dc}}{C} \quad (5)$$

Where η is the power conversion efficiency of GSVSC; u_{dc2} is the dc side voltage of GSVSC; i_{dc} is the dc current in the transmission cable; C is the equivalent dc capacitance. The corresponding equivalent ac and dc side circuits of GSVSC are shown in Fig. 3.

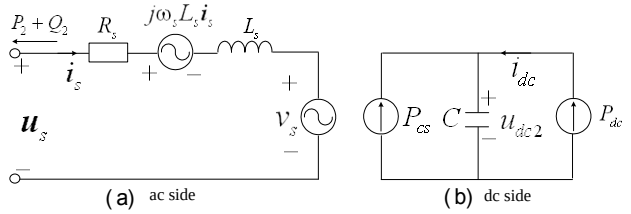

Fig. 3. Equivalent circuits for ac and dc side of GSVSC.

3 New control design for DFIG wind farm with VSC-HVDC integration

3.1 Control design for DFIG wind farm

As a wind farm is usually composed of tens or hundreds of individual wind generators, the control design for a wind farm is a fine and complex work. An adequate and reasonable aggregated model of wind farm is required because a detailed multi-generator model requires excessive time for simulation study. Although there are many different ways to equivalent a wind farm, the lumped wind farm model used in [6] is chosen for simplifying the whole system, as the major point of this study is not on this part. The control design for the lumped DFIG wind farm is based on stator oriented vector control and a MPPT control strategy is introduced to the rotor side converter for the maximum utilization of wind energy while the gird side converter is to regulate the dc link voltage. As their control strategies have been well documented [17-19], no more detailed description is given here.

3.2 Control design for WFVSC

The WFVSC is responsible for collecting the power generated by the wind farm when the wind farm is with VSC-HVDC integration. Moreover, it is also in charge of the wind farm ac voltage to provide a constant ac voltage. From this point of view, the WFVSC is more like a stiff voltage source for the wind farm, and works as a slack node in the whole system as it automatically absorbs the power sending from the wind farm regardless of active or reactive power. In addition, the frequency control can be introduced into the WFVSC control design, which will in turn impact the slip of the DFIG connected to the wind-farm-side voltage bus. This will be able to add in to the WFVSC power regulation under some special condition as describe in [6]. However, if there is a local load connected to the wind farm, frequency variation must be confined to a certain range, and its participation in power regulation ability is restricted. As the effect of the local load variation on the control strategy is considered in following study, so that the frequency control is not additionally included.

The equivalent circuit of WFVSC, as shown in fig. 2, indicates that the wind farm voltage $\boldsymbol{u}_w$ is indirectly established by $\boldsymbol{v}_w$, the ac side voltage of WFVSC. In order to improve wind farm dynamic voltage performance and reduce the impact of system impedance variation on the wind farm

voltage control, a dynamic voltage control block with a cross-product terms of d-q currents is introduce to the steady-state voltage control block. Due to the cross-product terms of d-q currents, the wind farm voltage dynamic response and insensitivity to the variation of the impedance between the wind farm and the WFVSC have improved effectively. However, this control structure is based on vector control, an appropriate coordinate orientation is very important for the decoupling control of d-q components of wind farm voltage. In general, there is a constant grid voltage to choose as the coordinate orientation. But, the wind farm voltage is very different, which is indirect established by the ac side voltage of WFVSC as previously discussed. Hence, a virtual voltage coordinate orientation should be decided before the wind farm voltage established. Since the ac side voltage of WFVSC is early established, the synchronous d-q axis is assumed oriented to the vector $\boldsymbol{v}_w$. Hence, the virtual d-q components of $\boldsymbol{v}_w$ can be decided as: $v^*_{wd}=v_w$, $v^*_{wq}=0$. Which will be the basic virtual control efforts for the WFVSC, and the predetermined value is defined as $v^*_{wd}=v^0_w$. Moreover, the wind farm frequency is set as 50Hz, which will be used in the d-q coordinate transformation.

Under the selected d-q axis, u_{wd}, u_{wq} the d-q components of $\boldsymbol{u}_w$ can be correspondingly decided. Since the control target is the constant wind farm voltage, which indicates that the synthesis value of u_{wd} and u_{wq} is constant. In order to realize the constant wind farm voltage control, a new control scheme is designed, which consists two parts: a steady-state voltage control block and a dynamic voltage control block. These two control blocks separately output the control efforts regulation of WFVSC, (v^1_{wd}, v^1_{wq}) and (v^2_{wd}, v^2_{wq}), which are correspondingly to the steady-state and dynamic control of wind farm voltage. Moreover, the synthesis of (v^1_{wd}, v^1_{wq}) and (v^2_{wd}, v^2_{wq}) are the total regulation control efforts of WFVSC, Δv_{wd} and Δv_{wq}, which will be add on the basic virtual d-q control efforts v^*_{wd} and v^*_{wq} to get the final control efforts of WFVSC. The following part will be the detail control efforts design.

For the steady-state voltage control block, according to the equation (2), the output control efforts regulation are given as

$$\begin{cases} v^1_{wd} = u^*_{wd} - R_w i^*_{wd} + \omega_w L_w i^*_{wq} \\ v^1_{wq} = u^*_{wq} - R_w i^*_{wq} - \omega_w L_w i^*_{wd} \end{cases} \tag{6}$$

Where, v^*_{wd} and v^*_{wq} are the d-q components of reference wind farm voltage $\boldsymbol{u}^*_w$; i^*_{wd} and i^*_{wq} are the outputs of proportional-integral controller for the u^*_{wd} and u^*_{wq}, which are given as

$$\begin{cases} i^*_{wd} = k_{p1}(u^*_{wq} - u_{wq}) + k_{i1}\int (u^*_{wq} - u_{wq})\mathrm{d}t \\ i^*_{wq} = -k_{p1}(u^*_{wd} - u_{wd}) - k_{i1}\int (u^*_{wd} - u_{wd})\mathrm{d}t \end{cases} \tag{7}$$

For the dynamic voltage control block, a cross-product term of d-q currents is introduce in the output control efforts regulation to achieve the independent control of dynamic parts of $\boldsymbol{u}_w$, as its d-q components are cross coupling. The cross-product terms of d-q currents are given as:

$$\begin{cases} v^2_{wd} = -R_w i_{wd\_cross} + \omega_w L_w i_{wq\_cross} \\ v^2_{wq} = -R_w i_{wq\_cross} - \omega_w L_w i_{wd\_cross} \end{cases} \tag{8}$$

Where the i_{wd_cross} and i_{wq_cross} are given as:

$$\begin{cases} i_{wd\_cross} = k_{p2}(i^*_{wq} - i_{wq}) + k_{i2}\int (i^*_{wq} - i_{wq})\mathrm{d}t \\ i_{wq\_cross} = k_{p2}(i^*_{wd} - i_{wd}) + k_{i2}\int (i^*_{wd} - i_{wd})\mathrm{d}t \end{cases} \tag{9}$$

Hence, the final control efforts for WFVSC are given as:

$$\begin{cases} v_{wd} = v^*_{wd} + \Delta v_{wd} \\ v_{wq} = v^*_{wq} + \Delta v_{wq} \end{cases} \tag{10}$$

Where Δv_{wd}, and Δv_{wq} are the total regulation control efforts of WFVSC which are given as:

$$\begin{cases} \Delta v_{wd} = v^1_{wd} + v^2_{wd} \\ \Delta v_{wq} = v^1_{wq} + v^2_{wq} \end{cases} \tag{11}$$

And the corresponding schematic diagram of the proposed control scheme for WFVSC is shown in Fig. 4.

3.3 Control design for GSVSC

In the practical applications, the nominal line impedances are calculated according to the short-circuit capacity, and the line impedances will change along with the time because of intermittent wind power variation and transmission cable aging, which result in the system operating point shifting. And so does the DC capacitor parameters. Moreover, the outside interference factors are also bearing considerable impacts on the GSVSC operating performance. Therefore, it is necessary to consider all these uncertainty factors in the control design for the GSVSC, which affect the power quality of wind power feeding into the power grid system.

In order to introduce parameter variations and external disturbance variation of system to the

control design, the equation (3) and (5) should be rewritten in the form of new dynamic equation as:

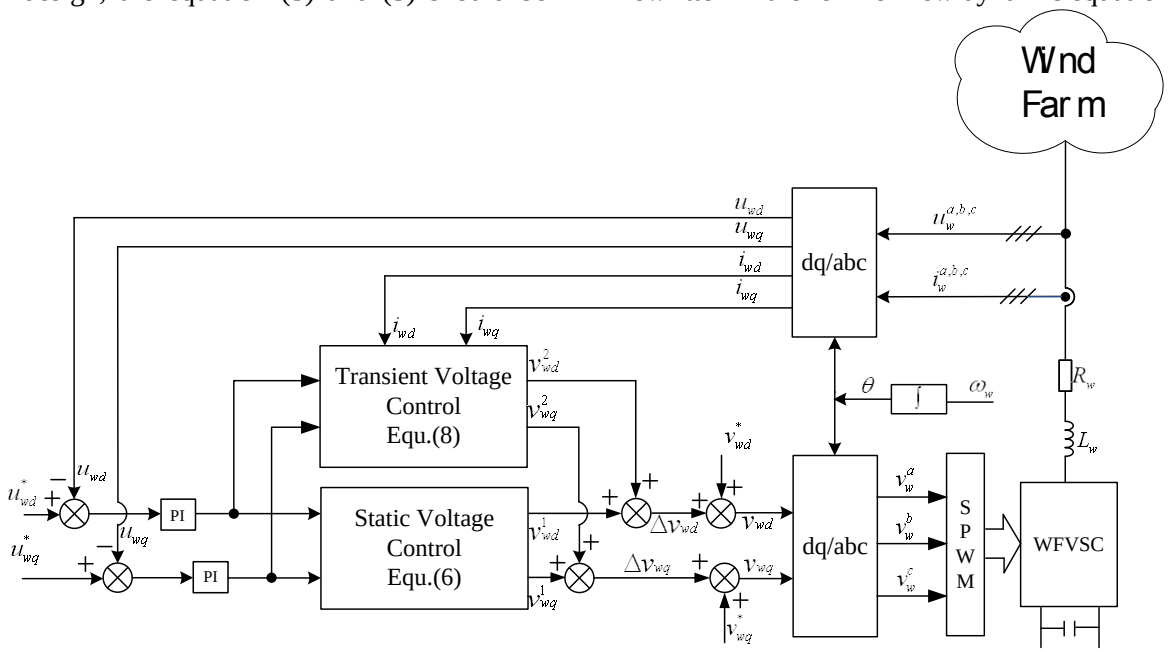

Fig. 4. Schematic diagram of the proposed control scheme for WFVSC.

$$\dot{\boldsymbol{x}} = -\mathrm{M}^{-1}\mathrm{B}\boldsymbol{x} - \mathrm{M}^{-1}\boldsymbol{l}_v + \mathrm{M}^{-1}(\mathrm{G}_s\boldsymbol{v}_s + \boldsymbol{u}_s) \quad (12\text{-a})$$

$$\dot{x}_3 = -\frac{1.5\eta u_{sd}x_1}{\bar{C}x_3} - \frac{1.5\eta u_{sq}x_2}{\bar{C}x_3} + \frac{i_{dc}}{\bar{C}} + l_{dc} \quad (12\text{-b})$$

Where $\boldsymbol{l}_v = \Delta\mathbf{M}\dot{\boldsymbol{x}} + \Delta\mathbf{B}\boldsymbol{x} + \boldsymbol{f}_0$ and $l_{dc} = [f_{dc} - \Delta C\dot{x}_3]/\bar{C}$ are the lumped uncertainties in the ac and dc side of GSVSC, which are the function of parameter variation and external disturbance. $\boldsymbol{f}_0$ and f_{dc} are respectively the ac and dc side external disturbance in practical applications. $\boldsymbol{x} = [x_1 \quad x_2]^T = [i_{sd} \quad i_{sq}]^T$; $x_3 = u_{dc2}$; $\boldsymbol{u}_s = [u_{sd} \quad u_{sq}]^T$; $\boldsymbol{v}_s = [v_{sd} \quad v_{sq}]^T$; $\mathbf{M} = \begin{bmatrix} \bar{L}_s & 0 \\ 0 & \bar{L}_s \end{bmatrix}$; $\boldsymbol{B} = \begin{bmatrix} \bar{R}_s & -\omega_s\bar{L}_s \\ \omega_s\bar{L}_s & \bar{R}_s \end{bmatrix}$; $\mathbf{G}_s = \begin{bmatrix} -1 & 0 \\ 0 & -1 \end{bmatrix}$; $\Delta\mathbf{M} = \begin{bmatrix} \Delta\bar{L}_s & 0 \\ 0 & \Delta\bar{L}_s \end{bmatrix}$; $\Delta\boldsymbol{B} = \begin{bmatrix} \Delta\bar{R}_s & -\omega_s\Delta\bar{L}_s \\ \omega_s\Delta\bar{L}_s & \Delta\bar{R}_s \end{bmatrix}$; $\bar{R}_s$, $\bar{L}_s$ and $\bar{C}$ denote the nominal values of R_s, L_s and C; $\Delta\bar{R}_s$, $\Delta\bar{L}_s$ and ΔC denote the introduced uncertainties of the ac and dc side parameters. Moreover, the bounds of the lumped uncertainties are assumed to be given by $\|\boldsymbol{l}_v\| < \rho_s$ and $|l_{dc}| < \rho_{dc}$, in which ρ_s and ρ_{dc} are given positive constants.

In the following part, an improved backstepping control scheme is designed for the GSVSC, which is depicted in the term of the product of sign function and the bounds of the lumped uncertainties with considering the parameter variations and external disturbance variation in the ac and dc side of GSVSC. The primary objective for this control design is to maintain the dc-side voltage of the GSVSC to be a predetermined value by balancing the transmitted active power between the dc side of the GSVSC and its ac side to the power grid. While, the other objective is reactive control design which is set to zero for the maximum usage of power converter. For decoupling the active and reactive powers control of the GSVSC, the vector control with synchronous d-q reference frame orientated to the power grid [16] is applied. That means $u_{sd}=U_s$, and $u_{sq}=0$. Where U_s is the amplitude of the power grid voltage. Based on the defined coordinate orientation, the backstepping control design for GSVSC is as follows:

Firstly, the tracking error of the dc bus voltage is defined as $e_{dc}=x_{3ref}-x_3$, where x_{3ref} is the reference of dc voltage. Then, a first Lyapunov function candidate is defined as $V_1=0.5e^2_{dc}$. According to (12-b), the derivation of V_1 with respect to time is correspondingly written as

$$\dot{V}_1 = e_{dc}\dot{e}_{dc} = e_{dc}(\dot{x}_{3ref} + \frac{1.5\eta u_{sd}x_1}{\bar{C}x_3} - \frac{i_{dc}}{\bar{C}} - l_{dc}) \quad (13)$$

A virtual control input is introduce as $\boldsymbol{x}$, and it's tracking error defined as $\boldsymbol{e}_s=\boldsymbol{\alpha}-\boldsymbol{x}$, which is stand for the control error of dq-axis currents of the power gird. Moreover, $\boldsymbol{\alpha}=[x_{1ref} \quad x_{2ref}]^T$, x_{1ref} and x_{2ref} are the respective reference commands. If x_{1ref} is designed as

$$x_{1ref} = -\frac{\bar{C}x_3}{1.5\eta u_1}[\dot{x}_{3ref} - \frac{i_{dc}}{\bar{C}} + k_0 e_{dc} + \rho_{dc}\,\mathrm{sgn}(e_{dc})] \quad (14)$$

Where k_0 is a positive constant, and sgn(·) is a sign function. Then, (13) can be rewritten as

$$\dot{V}_1 \le -\boldsymbol{e}^T \boldsymbol{K}_0 \boldsymbol{e} + \boldsymbol{e}_s^T \boldsymbol{C} \boldsymbol{e} \tag{15}$$

Where

$$\boldsymbol{e} = \begin{bmatrix} e_{dc} & 0 \end{bmatrix}^T ; \boldsymbol{K}_0 = \begin{bmatrix} k_0 & 0 \\ 0 & 0 \end{bmatrix}^T ; \boldsymbol{C} = \begin{bmatrix} -\dfrac{1.5 u_{sd}}{\bar{C} x_3} & 0 \\ 0 & 0 \end{bmatrix}^T .$$ K_0 is a given positive constant.

Since, reactive control design of GSVSC is set to zero for the maximum usage of power converter, x_{2ref} is designed as $x_{2ref}=0$.

According to (12-a), the derivation of $\boldsymbol{e}_s$ can be represented as

$$\begin{aligned} \dot{\boldsymbol{e}}_s &= \dot{\boldsymbol{x}}_{sref} - \dot{\boldsymbol{x}}_s \\ &= \dot{\boldsymbol{\alpha}} - \mathrm{M}^{-1}\mathrm{B}\boldsymbol{l}_v + \mathrm{M}^{-1}\boldsymbol{v}_s - \mathrm{M}^{-1}(\mathrm{G}_s \boldsymbol{v}_s + \boldsymbol{u}_s) \end{aligned} \tag{16}$$

Consider a second Lyapunov function candidate $V_2 = V_1 + 0.5\boldsymbol{e}_s^T \mathrm{M} \boldsymbol{e}_s$, and according to (15) and (16), its derivation with respect to time can be obtained as

$$\begin{aligned} \dot{V}_2 &= \dot{V}_1 + \boldsymbol{e}_s^T \dot{\mathrm{M}} \boldsymbol{e}_s / 2 + \boldsymbol{e}_s^T \mathrm{M} \dot{\boldsymbol{e}}_s \\ &\le -\boldsymbol{e}^T \boldsymbol{K}_0 \boldsymbol{e} + \boldsymbol{e}_s^T \boldsymbol{C} \boldsymbol{e} + \boldsymbol{e}_s^T \mathrm{M}[\dot{\boldsymbol{\alpha}} + \mathrm{M}^{-1}\mathrm{B} \\ &\quad + \mathrm{M}^{-1}\boldsymbol{l}_v - \mathrm{M}^{-1}(\mathrm{G}_s \boldsymbol{v}_s + \boldsymbol{u}_s)] \\ &\le -\boldsymbol{e}^T \boldsymbol{K}_0 \boldsymbol{e} + \boldsymbol{e}_s^T \boldsymbol{C} \boldsymbol{e} + \boldsymbol{e}_s^T (\mathrm{M}\dot{\boldsymbol{\alpha}} + \mathrm{B}\boldsymbol{x} \\ &\quad + \boldsymbol{l}_v - \mathrm{G}_s \boldsymbol{v}_s - \boldsymbol{u}_s) \end{aligned} \tag{17}$$

According to (17), the backstepping control efforts can be designed as:

$$\boldsymbol{v}_s = \mathrm{G}_s^{-1}[\mathrm{M}\dot{\boldsymbol{\alpha}} + \mathrm{CB} + \mathrm{K}_1 \boldsymbol{e}_s + \boldsymbol{u}_s + \rho_s \mathrm{sgn}(\boldsymbol{e}_s) + \boldsymbol{e}_s] \tag{18}$$

Where K_1 is a positive constant diagonal matrix.

In order to verify the control scheme is stable for GSVSC with the designed backstepping control efforts, and according to Lyapunov stability theorem [20], the system stability is proved as:

$$\begin{aligned} \dot{V}_2 &\le -\boldsymbol{e}^T \mathrm{K}_0 \boldsymbol{e} - \boldsymbol{e}_s^T \mathrm{K}_1 \boldsymbol{e}_s + \boldsymbol{e}_s^T \boldsymbol{l}_v - \left|\boldsymbol{e}_s^T\right| \rho_s \\ &\le -\boldsymbol{e}^T \mathrm{K}_0 \boldsymbol{e} - \boldsymbol{e}_s^T \mathrm{K}_1 \boldsymbol{e}_s + \left|\boldsymbol{e}_s^T\right| \left\|\boldsymbol{l}_v\right| - \left|\boldsymbol{e}_s^T\right| \rho_s \\ &\le -\boldsymbol{e}^T \mathrm{K}_0 \boldsymbol{e} - \boldsymbol{e}_s^T \mathrm{K}_1 \boldsymbol{e}_s - \left|\boldsymbol{e}_s^T\right| (\rho_s - \left|\boldsymbol{l}_v\right|) \\ &\le -\boldsymbol{e}^T \mathrm{K}_0 \boldsymbol{e} - \boldsymbol{e}_s^T \mathrm{K}_1 \boldsymbol{e}_s < 0 \end{aligned} \tag{19}$$

Since the derivative of V_2 is a negative-definite function, it can imply that $\boldsymbol{e}$ and $\boldsymbol{e}_s$ go to zero asymptotically. That means if the conditions of $\left\|\boldsymbol{l}_v\right\| < \rho_s$ and $\left|l_{dc}\right| < \rho_{dc}$ are satisfied, the stability of proposed backstepping control scheme can be guaranteed. Note that, the final backstepping control efforts for GSVSC is designed in term of the product of sign function and the bounds of the lumped uncertainties, which is playing a substantial role in resisting the variation of the uncertainties in ac and dc side of the GSVSC. Moreover, it reduces the chattering phenomena in the traditional backstepping control scheme and it also the key control improvement for the GSVSC. The corresponding control scheme for the proposed backstepping control design is shown in Fig. 5.

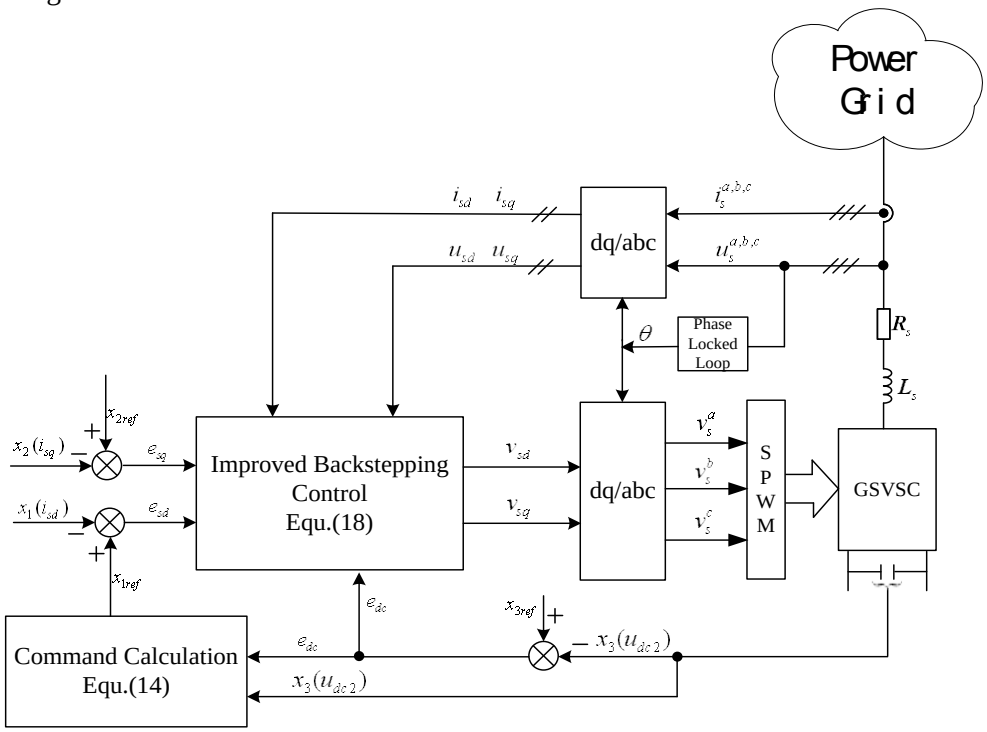

Fig. 5. Schematic diagram of the proposed improved backstepping control scheme for GSVSC.

4 Simulation studies and results

For evaluation of the proposed control strategy, numerical simulations have been carried out on Matlab/Simulink. The whole hypothetic network configuration of a DFIG wind farm with VSC-HVDC integration is constructed according to Fig. 1. It consists of a 200MW wind farm using DFIG wind turbines, which are connected to the power grid via a 200MW/±150kV VSC-HVDC. Details of the aggregated model of the lumped DFIG [21] wind farm are given in the appendix. Fig.6. shows the equivalent wind turbine power characteristics (Pitch angle=0 deg) and the MPPT curve.

As shown in Fig. 1, a local load of 50MW is used to test its impact on the performance of the system with the proposed control strategy. The wind-farm-side VSC (WFVSC) and grid-side VSC (GSVSC) are three-level neutral point clamped converters, which result in a smaller power loss in comparison with conventional two-level converters [6]. The dc cable transmission line is 100km in length, with two 35μF dc link capacitors at its two ends. The corresponding time constant for individual capacitor is set at 8ms, so that small voltage ripple and favourable performance in response to power changing can be achieved [22].

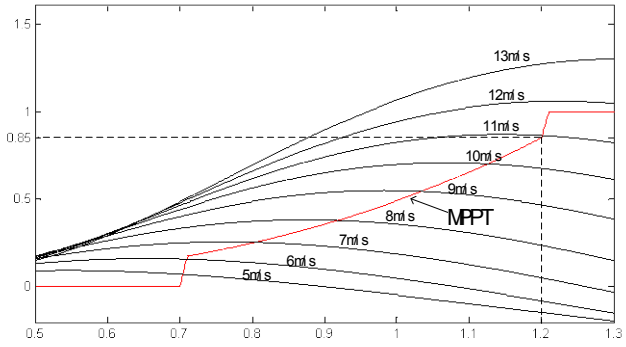

Fig. 6. Equivalent wind turbine power characteristics (Pitch angle=0 deg) and the MPPT curve for DFIG.

The switching frequency for the VSC is set at 1.35kHz. The corresponding harmonic frequencies are 2.7kHz and its multiples, which can be filtered out by ac filters at two ends of the VSC-HVDC. A transformer T1 with 690V/110kV is used for the WFVSC connection, while a transformer T2 with 110kV/230kV is used for the GSVSC connection. Some other nominal system parameters are also given in the appendix.

In order to illustrate the merit of the proposed control strategy for the DFIG wind farm with VSC-HVDC grid integration, three different kinds of simulation cases are introduced in this study. The factors of system parameter variation of ac and dc transmission impedance and dc capacitance are considered for the simulation cases design, and so does the variation of the local load and power gird voltage. The corresponding simulation cases and simulation results are depicted as follows:

Case 1: Wind speed increases from 8m/s to 13m/s at 1s, and then decreases to 11 m/s at 3s, without introducing any variation or disturbance to the parameters of WFVSC and GSVSC.

Case 2: Wind speed is set at 11m/s, while the equivalent ac side impedance of WFVSC increase by 20% while there is no variation or disturbance on the parameters of GSVSC. Moreover, an external disturbance voltage composed of a 0.2p.u. amplitude plus 3rd harmonic frequency is injected into the power grid during 1s-3s.

Case 3: Wind speed is set at 11m/s, while the equivalent ac side impedance and dc side capacitance of GSVSC increase by 20% while there is no variation or disturbance on the parameters of WFVSC. And under this condition, a local load of 50MW active power at the wind farm side cuts into the wind farm gird at 1s and then cuts off again at 3s.

The simulations results of the proposed control strategy under the three different cases are depicted in Figs. 7 respectively. In each case, the subfigure of same location has same representation. The subfigure (a) is the active of WFVSC in pu and wind speed (m/s); the subfigure (b) is the wind farm voltage in pu; the subfigures (c) is the wind farm voltage at the special time; the subfigure (d) is the frequency of wind farm; the subfigure (e) and (f) are the dc voltage of WFVSC and GSVSC in pu; the subfigure (g) is the active and reactive power of GSVSC in pu; the subfigure (h) is the improved backstepping control efforts for GSVSC in pu; the subfigure (i) is the power grid voltage and current of phase A, and the subfigure (j) is the power grid voltage and current of phase A at the special time.

As seen in Fig. 7(b-d), the designed controller for WFVSC can effectively maintain the wind farm voltage to the predetermined value even though there are fluctuations in the wind speed, local load and transmission parameters. And so does the frequency of the wind farm. As seen in Fig. 7(e-g), the dc voltage and reactive power of GSVSC is also well controlled to the command values even though there are parameters variation and external

disturbance in the ac and dc side of the GSVSC. The simulation results also reveal that the disturbances of wind farm side and the power grid side do not have any impact on the performance of the counterpart controller. Finally, Figs. 7(i) and (j)

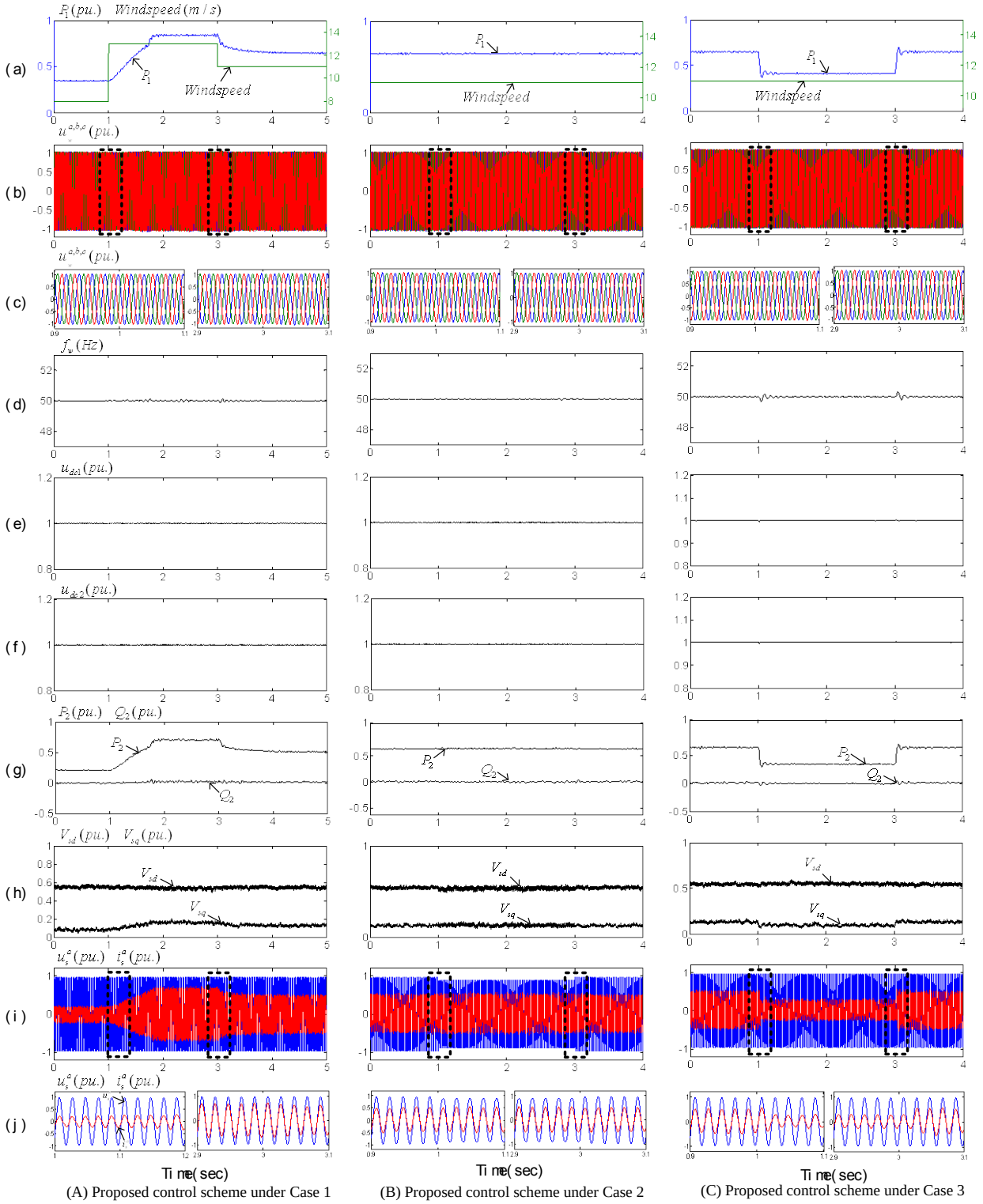

(A) Proposed control scheme under Case 1 (B) Proposed control scheme under Case 2 (C) Proposed control scheme under Case 3

Fig. 7. Simulation results of the DFIG wind farm with VSC-HVDC under the three different simulated cases, (a) active power of WFVSC (pu) and wind speed (m/s), (b) wind farm voltage (pu), (c) wind farm voltage at the special time (pu), (d) frequency of wind farm (Hz), (e) dc voltage of WFVSC (pu), (f) dc voltage of GSVSC (pu), (g) active and reactive power of GSVSC (pu), (h) improved backstepping control efforts for GSVSC (pu), (i) power grid voltage and current of phase A (pu), (j) power grid voltage and current of phase A at the special time (pu).

show that the power gird voltage and current are in phase even though there are parameters variations and external disturbances in the ac side of the GSVSC, which means the power quality of the grid can reach a satisfactory outcome in all the simulation cases.

5 Discussions and Conclusions

This paper has demonstrated a new designed control strategy for a DFIG wind farm with VSC-HVDC integration. The new control strategy consists two independent parts for WFVSC and GSVSC which are separately designed. Numerical simulations carried on MATALB/Simulink verify that the proposed control strategy is of satisfied performance. The major contributions of this study can be summarized as follows: 1) A new control scheme for WFVSC is designed, which is based on vector control system with a virtual voltage orientation. Moreover, a cross-product term of d-q currents is introduced, which not only improves the system control response but also reduces the influence from the variation of system parameters. 2) A modified model with considering the ac/dc-side parameters variation and external disturbance for GSVSC is derived. 3) An improved backstepping control scheme is proposed according to the modified model. The key control improvement is the introduction of a term with the product of sign function and the lumped uncertainties, which reduces the chattering phenomena in the traditional backstepping control scheme. Moreover, the stability of the improved control scheme is also proved with the Lyapunov stability theorem. 4) The proposed control strategy is a robust control scheme which not only improves the power quality of the grid but also strengthens the reliable operation of the wind farm, even though there are parameter variations and external disturbances.

Appendix

Simulation system parameters:

- Parameters for the aggregated model of the lumped DFIG wind farm:

Ratings: S_n=200MW, f_n=50Hz, U_n=690V (Line voltage rms);
Stator resistance: 0.0060pu;
Stator leakage inductance: 0.0624pu;
Rotor resistance: 0.0099pu;
Rotor leakage inductance: 0.0752pu;
Magnetizing inductance: 3.97pu;
Inertia constant H: 1s.

- T1 transformer parameters

Ratings: S_n=250MW, f_n=50Hz;
Primary windings: 690V-Yg;
Secondary windings: 110kV-Δ;
Short circuit impedance: Z_T=0.0025+j0.075pu;

- T2 transformer parameters

Ratings: S_n=250MW, f_n=50Hz;
Primary windings: 110kV-Δ;
Secondary windings: 230kV-Yg;
Short circuit impedance: Z_T=0.0025+j0.075pu;

- Wind farm and grid side converter parameters:

Reactor: L=23.9mH, R=75mΩ;
DC-link capacitor: 35μF;

Acknowledgment: This research work is supported by Technical Plan Key Project of Chongqing Science and Technology Commission (Grant No.2008AB3047).

References:

[1] Z. Chen, F. Blaabjerg, Wind farm-A power source in future power systems, *Renewable and Sustainable Energy Reviews*, Vol.13 No. 6, 2009, pp.1288-1300.

[2] H. Li, C. Yang, B. Zhao, H.S. Wang, Z. Chen, Aggregated models and transient performances of a mixed wind farm with different wind turbine generator systems, *Electric Power Systems Research*, Vol.92 November, 2012, pp 1-10.

[3] S. Cole, R. Belman, Transmission of bulk power, *IEEE Transactions on Industrial Electronics*, Vol.3 No. 3, 2009, pp. 19-24.

[4] D. Xiang, L. Ran, P. J. Tavner, S. Yang, Control of a doubly fed induction generator in a wind turbine during grid fault ride-through, *IEEE Trans. on Energy Conversion*, Vol. 21, No. 3, September 2006, pp. 652-662.

[5] H. Zhou, G. Yang, J. Wang, and H. Geng, Control of a hybrid high-voltage DC connection for large doubly fed induction generator-based wind farms, *IET Renewable Power Generation*, Vol. 5, No. 1, 2011, pp. 36-47.

[6] L. Xu, L. Yao, C. Sasse, Grid integration of large DFIG-based wind farms using VSC transmission, *IEEE Transactions on Power Systems*, Vol. 22, No. 3, 2007, pp. 976-984. Vol. 8, No. 2, 2009, pp. 217-225.

[7] N. Flourentzou, V. G. Agelidis, G. D. Demetriades, VSC-based HVDC power

transmission systems: An overview, *IEEE Transactions on Power Electronics*, Vol. 24, No 3, 2009, pp. 592-602.

[8] H. S. Ramadan, H. Siguerdidjane, M. Petit, and R. Kaczmarek, Performance enhancement and robustness assessment of VSC-HVDC transmission systems controllers under uncertainties, *Electrical Power & Energy Systems*, Vol. 35, No. 1, 2012, pp. 34-46.

[9] A. R. Årdal, *Feasibility Studies on Integrating Offshore Wind Power with Oil Platforms*, Master Thesis, available: http://daim.idi.ntnu.no/soek/, Department of Electrical Engineering, NTNU, 2011.

[10] S. Li, Z. Wang, G. Wang, D. Wu, PID Neural Network Sliding-mode Controller for Three-level Offshore Wind Power VSC-HVDC Converter, *Proceedings of the CSEE*, Vol. 32, No. 4, 2012, pp. 20-28.

[11] H. Chen, *Control and protection of VSC based HVDC system under AC system fault conditions*, Doctor Thesis, Zhejiang University, 2007.

[12] M. Durrant, H. Werner, K. Abbott, Synthesis of multi-objective controllers for a VSC HVDC terminal using LMIs, *Proc. of the 43rd IEEE Conference Decision and Control*, 2004, pp. 4473-4478

[13] S. Y. Ruan, G. J. Li, X. H. Jiao, Y. Z. Sun, T. T. Lie, Adaptive control design for VSC-HVDC systems based on backstepping method, *Electric Power Systems Research*, Vol. 77, No. 6, 2007, pp. 559-565.

[14] R. J. Wai, J. D. Lee, Backstepping-based levitation control design for linear maglev rail system, *IET Control Theory & Applications*, Vol. 2, No. 1, 2008, pp. 72-86.

[15] A. Karimi, A. Feliachi, Decentralized adaptive backstepping control of electric power system, *Electric Power Systems Research*, Vol. 78, No. 3, 2008, pp. 484-493.

[16] L. Xu, B. R. Andersen, P. Cartwright, VSC transmission operating under unbalanced ac conditions – Analysis and control design, *IEEE Transactions on Power Delivery*, Vol. 20 No. 1, 2005, pp. 427–434.

[17] J.J. Zhao, X. Li, J.T. Hao, Voltage control scheme in distribution network with double feed induction generator wind farm, *WSEAS Transactions on Circuits and Systems*, Vol. 8, No. 8, 2009, pp. 709-718.

[18] H. K. Jafari, Simulation of doubly-fed machine with improved wind turbine, *WSEAS Transactions on Circuits and Systems*, Vol. 8, No. 2, 2009, pp. 217-225.

[19] J. Smajo, Electromagnetic torque analysis of a DFIG for wind turbines, *WSEAS Transactions on Systems*, Vol. 7, No. 5, 2008, pp. 479-488.

[20] K. J. Astrom, B. Wittenmark, *Adaptive Control*. New York: Addison-Wesley, 1995.

[21] H. Li, M. Zhao, B. Zhao, Fault diagnosis methods for key sensors of doubly fed wind turbine, *Proceedings of the CSEE*, Vol. 31, No. 6, 2011, pp. 73-78.

[22] C. Du, M. Bollen, E. Agneholm, A. Sannino, A new control strategy of a VSC HVDC system for high-quality supply of industrial plants, *IEEE Transactions on Power Delivery*, Vol. 22, No. 4, 2007, pp. 2386-2394.